Experimental Validation of the Performance of a Microreactor for the High-Throughput Screening of Catalytic Coatings

ARTICLE *in* INDUSTRIAL & ENGINEERING CHEMISTRY RESEARCH · MARCH 2007

Impact Factor: 2.59 · DOI: 10.1021/ie061081w

6 AUTHORS, INCLUDING:

Evgeny V. Rebrov
The University of Warwick
173 PUBLICATIONS **1,726** CITATIONS
SEE PROFILE

Chris R. Kleijn
Delft University of Technology
168 PUBLICATIONS **1,740** CITATIONS
SEE PROFILE

Experimental Validation of the Performance of a Microreactor for the High-Throughput Screening of Catalytic Coatings

M. J. M. Mies,[†] E. V. Rebrov,[†] L. Deutz,[‡] C. R. Kleijn,[‡] M. H. J. M. de Croon,[†] and J. C. Schouten*,[†]

Department of Chemical Engineering and Chemistry, Eindhoven University of Technology, P.O. Box 513, 5600 MB Eindhoven, The Netherlands, and Department of Multi-Scale Physics, Delft University of Technology, Prins Bernhardlaan 6, 2628 BW Delft, The Netherlands

In this paper, the results of computational fluid dynamics simulations of flow, temperature, and concentration distributions used in the design of a microreactor for the high-throughput screening of catalytic coatings (Mies et al., *Chem. Eng. J.* **2004**, *101*, 225) are compared with experimental data, and good agreement is obtained in all cases. The experimental results on flow distribution were obtained from laser Doppler anemometry measurements in the range of Reynolds numbers from 6 to 113. The measured flow nonuniformity in the separate reactor compartments was below 2%. The temperature distribution was obtained from thermocouple measurements. The temperature nonuniformity between the reactor compartments was below 3 K at a maximum heat production rate of 1.3 W in ethylene oxidation at 425 °C over $CuO/Al_2O_3/Al$ coatings. With respect to concentration gradients, a deviation from the average rate of reaction of only 2.3% was obtained at realistic process conditions in the ethylene ammoxidation process over identical Co−ZSM-5 coatings in all reactor compartments. The cross talking noise between separate compartments does not exceed 0.1% when the reactor parts have a smooth surface finish. This illustrates the importance of ultraprecision machining of surfaces in microtechnology, when interfaces cannot be avoided.

1. Introduction

Structured[1] and microstructured reactors[2,3] are more and more recognized for their unique properties and potential applications in chemistry and the chemical process industry. They are particularly suited for highly exothermic and fast reactions allowing temperature control and isothermal operation. The efficient use of (micro)structured catalytic reactors requires a shaping of the catalyst usually by deposition of thin catalytic coatings at the walls of the reactor channels. Over the past decade, many methods have been developed or considerably improved to deposit catalytic coatings on a substrate: zeolite hydrothermal synthesis,[4−8] anodic oxidation,[9−11] electrophoretic deposition,[12] sol−gel synthesis,[13−16] washcoating,[17] atomic layer deposition,[18−20] several vapor deposition techniques,[21,22] and electrochemical depositions in ionic melts.[23,24] The choice of the deposition method depends on the size of the coated substrate, scale of substrate structurization, and the properties of the substrate and the active component.

The development of novel and superior catalytic coatings for structured reactors is often an empirical process, which is based on conventional catalyst know-how and common sense. Therefore, high-throughput testing (HTT) of libraries of coatings for desired catalytic properties is required at realistic process conditions to speed up this development and optimization trajectory. Moreover, HTT can be used for the primary screening of large coating libraries to discover new potential candidates for a specific chemical process. Microstructured reactors can be used as a tool for the high-throughput screening of catalytic coatings and for kinetic studies.[25] However, it is not straightforward to obtain identical process conditions in a large number of microchannels, due to the nonuniformity of the fluid flow distribution in the microchannels at a low pressure drop. Therefore, a three-dimensional design of the full reactor is often required before its fabrication and assembling. Especially, flow equalization between different channels and temperature uniformity are of importance. In our previous study,[25] we proposed a high-throughput microreactor (HTMR) for the screening of eight different catalytic coatings with turnover frequency values of 0.1−10 s^{-1} in a flow range of 50−1000 mL min^{-1}. The flexibility in the flow rate allows the testing of catalytic coatings in the differential reactor mode, which considerably simplifies the interpretation of the kinetic data. In this reactor design, the geometries of the low-pressure drop flow distributor and the gas sampling section were optimized using the computational fluid dynamics (CFD) code Fluent.[25] We proposed an original design of a flow distribution header, consisting of a cone diffuser and a thick-walled screen for equalizing the flow distribution in microstructured reactors.[25−28] The influence of the different design parameters of a thick-walled screen on the flow nonuniformity has been analyzed. According to the CFD study, the degree of flow nonuniformity does not depend on the flow distribution entering the thick-walled screen and is defined by the geometry of the thick-walled screen itself. The proposed screen configuration can minimize the ratio of the maximum flow velocity to the minimum flow velocity from 2 (without the screen) to 1.005 (with the screen) for a wide range of Reynolds numbers, which in turn can improve the performance of a downstream microreactor.[29]

In the present paper, an experimental validation study is performed to compare the performance of the HTMR versus the design criteria, namely, the flow distribution in the separate reactor compartments, the temperature distribution, and the accuracy of sampling of the product gases. The flow distribution was studied using laser Doppler anemometry (LDA), which is a direct method for the determination of the fluid velocity in the separate microstructured compartments, while it does not

* To whom correspondence should be addressed. Tel.: +31 40 247 2850. Fax: +31 40 244 6653. E-mail: j.c.schouten@tue.nl. URL: www.chem.tue.nl/scr.

[†] Eindhoven University of Technology.

[‡] Delft University of Technology.

10.1021/ie061081w CCC: $27.50
Published on Web 03/21/2007 **PAGE EST: 9.4**

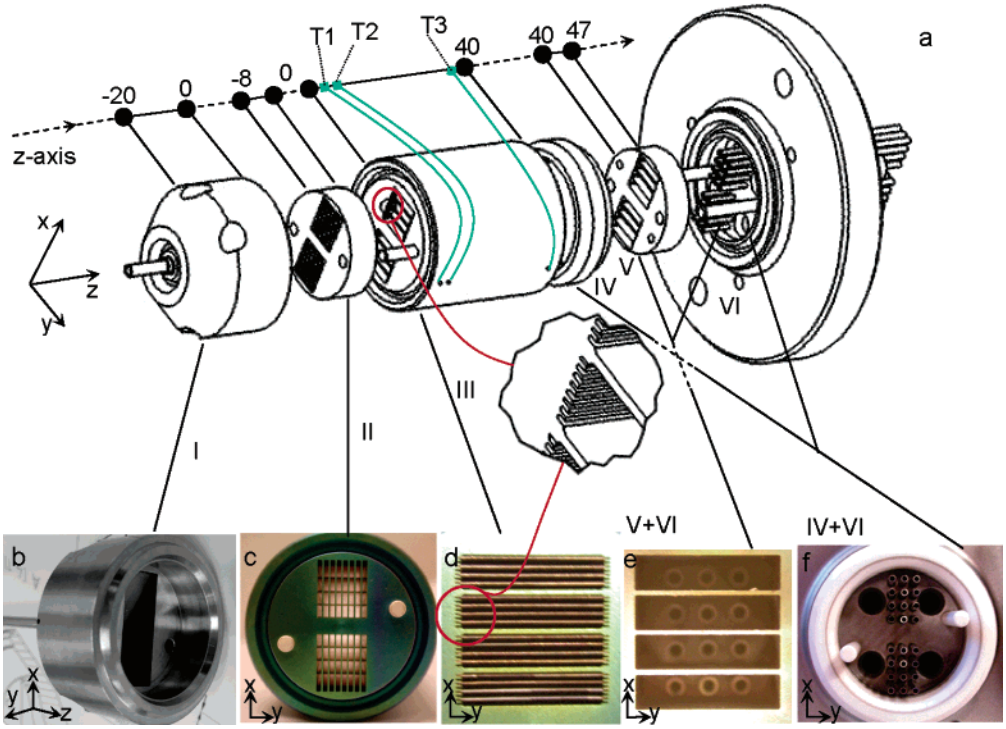

Figure 1. (a) A schematic illustration of the high-throughput microreactor, which comprises a cone diffuser (I), a thick-walled screen (II), eight reactor compartments (III), an insulating ring (IV), an outlet flow confusor (V), and a sampling section (VI). The dimensions and coordinates are indicated above the figure along the *z* axis. The axial positions of the thermocouples are indicated with T1, T2, and T3. The inset of the HTMR compartment shows the eight microstructured cavities in the side wall along the length of the reactor. (b) The cone diffuser (I), is connected upstream to the inlet capillary (o.d. = 3 mm, i.d. = 2.16 mm). (c) The thick-walled screen (II, $z = -8$ mm), consisting of two series of eight elongated channels, which are positioned with a 90° turn relative the reactor compartments (III). The walls of reactor compartments are also visible through the open areas of the screen. (d) The upper four reactor compartments (III, $z = 0$ mm), which are loaded with four catalytic coatings per compartment. (e) The upper four compartments of the outlet flow confuser (V, $z = 40$ mm), which are aligned with the corresponding reactor compartments (III). Three sampling capillaries (VI) are positioned at 4 mm inside every compartment outlet. (f) The sampling and outlet section (VI) and the ceramic ring (IV), which separates the hot and cold HTMR parts. The eight sets of three sampling capillaries as well as the four common reactor outlets are visible. The two ceramic pins are for HTMR assembling purposes. The dimensions of the various reactor sections in parts b−f are indicated in Figures 1a, 2, and 4.

disturb the fluid flow. Especially, the accuracy in the measurement itself, as well as in the positioning of the relatively small measurement volume with respect to the channel outlets, makes the LDA technique a powerful tool for fluid flow analysis in microstructured devices. The temperature distribution was measured by means of thermocouples. In addition, the concentration distribution was investigated at real process conditions in the ethylene ammoxidation process over zeolitic catalytic coatings.

2. Experimental

2.1. High-Throughput Microreactor. The HTMR (Figure 1a−f) comprises a cone diffuser, upstream connected to the inlet capillary (i.d. = 2.16 mm) (I), a thick-walled screen (II), eight reactor compartments (III), an insulating ring (IV), an outlet flow confusor (V), and a sampling section (VI). Eight cavities of $130 \times 400\ \mu m^2$ were microfabricated by electrical discharge machining in the side walls of each reactor compartment along the length of the reactor (Figure 2). In this way, each reactor compartment can be loaded with up to eight substrate plates with catalytic coatings. The center of the coordinate system ($x = 0$, $y = 0$, and $z = 0$) is on the center axes at the interface between the screen (II) and the reactor (III) (Figures 1a and 2). To monitor axial and radial temperature gradients, thermocouple T1 is positioned close to the external surface ($x = 14$ mm and $z = 3$ mm) and two thermocouples (T2 and T3) are positioned along the center axis at $z = 3$ and 37 mm, respectively. A band heater with a maximum power output of 300 W was used for the temperature control of the reactor and was positioned at its surface from $z = 5$ to 43 mm (not shown in Figure 1a). In the plane of the cross-section of the screen (II), two sets of eight elongated channels are positioned with a 90° turn relative to the reactor compartments. The screen distributes the flow equally over the reactor compartments and simultaneously preheats the inlet gas flow to the reaction temperature. Sections V and VI were maintained at 120 °C. The main part of the outlet gas flow (ca. 99.5 vol %) is directed to the four common outlets (i.d. = 6 mm, VI). The sampling section (VI) comprises eight sets of three capillaries (i.d. = 1.0 mm, o.d. = 1.2 mm), that is, three capillaries per compartment, positioned at 4 mm inside the flow confusor (V). A total of 0.5 vol % of the total flow is selected for product analysis by a multipositional valve. Isokinetic suction intake was maintained by a diaphragm micropump. Sequential analysis of the product gases was automated via Lab-Jack software.

2.2. Flow Distribution. The fluid flow distribution in the HTMR compartments was investigated using LDA. At the low velocities and small measurement volumes of interest to the present study, LDA measurements in gas flows are complicated and not very accurate. For low velocity and (nearly) isothermal flows, however, the flow behavior is fully determined by the Reynolds number. This allows for the replacement of gas by a liquid as flowing medium, when the Reynolds number is kept fixed. Assembled sections I−III of the HTMR (see Figure 1a) were positioned in a water/PVP-K90 (polyvinylpyrolidone; $M_w = 1.0 \times 10^6$ to 1.5×10^6 g mol^{-1}) solution with the *z* axis parallel to the gravity vector. The gravitationally driven flow

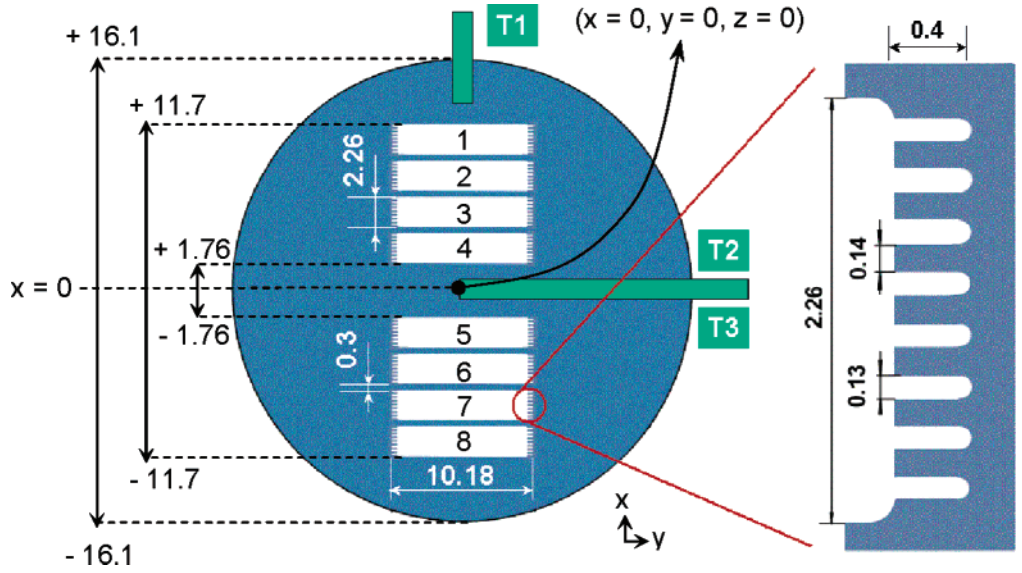

Figure 2. Cross-section of the microstructured reactor (III, $z = 0$ mm) with an enlarged view of the microstructures in the side wall of the compartment at the right-hand side. The radial positions of the thermocouples are indicated with T1, T2, and T3. The center of the coordinate system ($x = 0$, $y = 0$, and $z = 0$) is on the center axes at the interface between the screen (II) and the reactor (III).

Table 1. Fluid Flow Properties (water/PVP-K90) for the LDA Experiments

experiment no.:	1	2	3	4
$\bar{V}_{dwn}$, (mm s^{-1})	0.66 ± 0.02	1.17 ± 0.02	5.85 ± 0.05	9.71 ± 0.08
ϕ_v, (cm^3 s^{-1})	0.11 ± 0.01	0.20 ± 0.01	0.99 ± 0.01	1.65 ± 0.01
$\bar{v}_{cap}$, (mm s^{-1})	32 ± 1	59 ± 2	293 ± 10	485 ± 17
η, (mPa s)	9.5 ± 0.2	9.2 ± 0.2	9.0 ± 0.2	8.5 ± 0.2
Re_{cap}, (−)	6.7 ± 0.4	12.7 ± 0.4	64 ± 0.4	113 ± 0.4

of the solution through the HTMR was set at 0.11, 0.20, 0.99, and 1.65 cm^3 s^{-1} (STP). The properties of the fluid flow at the various flow conditions are given in Table 1. With these, the corresponding Reynolds numbers in the inlet capillary (Re_{cap}) were 6.7, 12.7, 64, and 113, respectively. The LDA analysis was performed at the outlets of the reactor compartments ($y = 0$ mm and $z = 40$ mm) along the x axis from $x = -11.7$ mm to $x = 11.7$ mm (Figure 2). Each traverse along the x axis consisted of LDA analysis at 133 positions. At each position, 20 480 LDA measurements were performed, from which both the average velocity at that position and its standard deviation were determined.

LDA measurements were performed in forward scatter, reference beam mode[30] (Figure 3), using a diode-pumped 532 nm green laser and a frequency shift of 20 kHz. No tracer particles were added to the water/PVP-K90 solution, as the fluid already contained sufficient natural seeding. The size of the cigar-shaped measurement volume was 1.19 × 0.22 × 0.22 mm^3. The measurement volume was positioned at a distance less than 1.0 mm from the outlets of the reactor compartments, with its longitudinal axis parallel to the longitudinal axis of the compartments in the y direction, and thus perpendicular to the axial velocity profile in the z direction. In this way, the location uncertainty in the velocity measurement data was reduced as much as possible (Appendix I). The LDA signal was processed by means of an IFA550 signal processor. Velocity bias was corrected for by means of the time between data correction method.[31]

2.3. Temperature Distribution. The temperature distribution in the HTMR was determined in ethylene oxidation

$$C_2H_4 + 3O_2 \rightarrow CO_2 + 2H_2O$$
$$\Delta H^0_{698K} = -1284 \text{ kJ mol}^{-1} \quad (1)$$

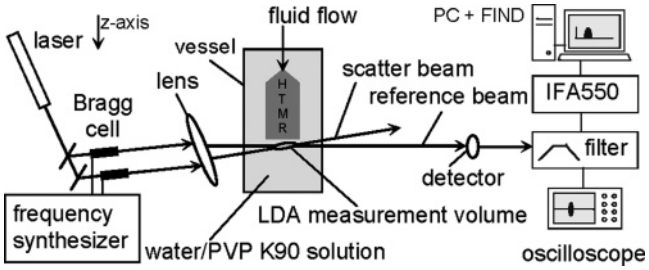

Figure 3. Schematic overview of the LDA setup.

on CuO/Al_2O_3/Al coatings at 425 °C with an ethylene concentration of 2 vol % and an oxygen concentration of 0.5−12 vol % in helium at a total flow of 250 mL min^{-1}. The evolved reaction heat was calculated from the CO_2 concentration in the effluent gas flow with the following equation:

$$Q = \frac{0.5 y_{CO_2} F_v \Delta H^0_{698K}}{V_m} \quad (2)$$

where Q is the produced reaction heat (W), y_{CO_2} is the mole fraction of carbon dioxide, F_v is the total flow rate at STP conditions (m^3 s^{-1}), V_m is the gas molar volume (m^3 mol^{-1}), and ΔH^0_{698K} is the reaction enthalpy (J mol^{-1}).

Al_2O_3 coatings were prepared by the anodic oxidation of aluminum substrates of 40 × 9.8 mm^2 with a thickness of 0.09 mm (99.99 wt.%; Goodfellow Cambridge Limited). A total of 12 aluminum plates per batch were oxidized simultaneously in a cylindrical 20 L electrolysis vessel. The preparation conditions are explained in detail elsewhere.[11] A 15 μm alumina layer was produced under current control conditions with an anodic current density of 15 mA cm^{-2} in an aqueous 10 wt % oxalic acid solution at 3 °C for 2 h under continuous stirring at 180 rpm. CuO/Al_2O_3/Al coatings were prepared by wet impregnation of the alumina layer by a 2.5 M aqueous copper nitrate solution for 1 h at 20 °C. The excess of the impregnation solution was wiped of the plates with tissue paper. The plates were calcined at 400 °C for 1 h in air at a flow of 100 mL min^{-1}. The CuO loading was 2.3 wt % of the mass of Al_2O_3, where the apparent density of the alumina layer is 2.0 g cm^{-3}.

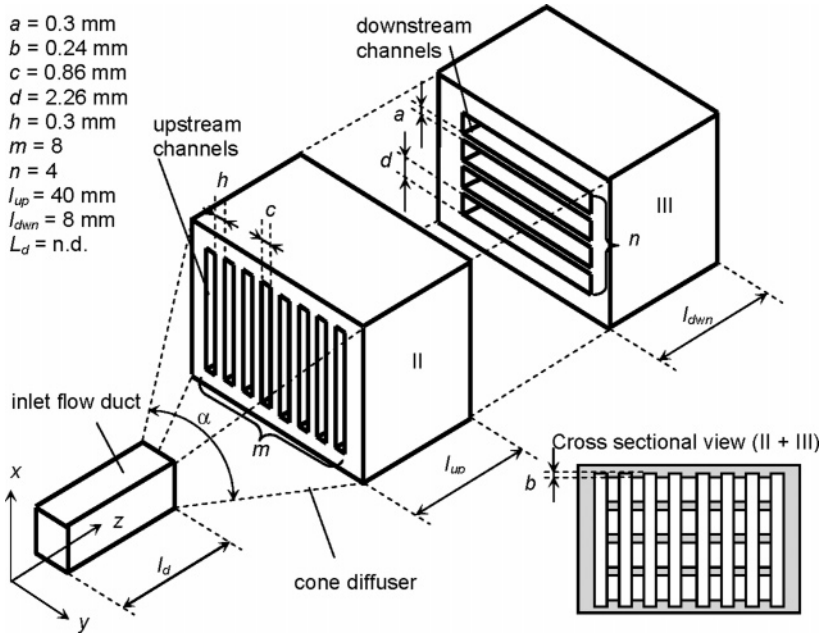

Figure 4. Header consisting of a cone diffuser and a thick-walled screen positioned in front of the microreactor. Due to symmetry, only half of the geometry is modeled. The upstream section (II) comprises a set of eight elongated parallel upstream channels, and the microreactor (III) comprises a set of four elongated parallel downstream channels positioned at an angle of 90° with respect to the upstream channels. Parameter *a* is the minimum length between two neighboring downstream channels; parameter *b* is the distance in cross-sectional view between a top wall of the first downstream channel and a side wall of the upstream channels. Parameter *c* is the width of the upstream channels. Parameter *d* is the height of the downstream channels. Parameter *h* is the distance between the neighboring upstream channels. Parameters l_{up} and l_{dwn} are the lengths of upstream and downstream channels of the screen, respectively.

2.4. Concentration Distribution. The concentration distribution at process conditions was determined in ethylene ammoxidation

$$C_2H_4 + NH_3 + O_2 \rightarrow CH_3CN + 2H_2O \qquad \Delta H^0_{698K} = -418 \text{ kJ mol}^{-1} \quad (3)$$

on Co−ZSM-5 coatings at 425 °C at equimolar oxygen, ethylene, and ammonia concentrations of 4 vol % in helium at a total flow of 250 and 500 mL min^{-1}, respectively. Blank experiments were carried out on inert titanium plates to exclude the contribution of the reactor material to reactant conversion. Prior to the experiments, the $CuO/Al_2O_3/Al$ and Co−ZSM-5 coatings were pretreated in helium for 1 h at 450 and 500 °C, respectively.

ZSM-5 coatings were prepared via hydrothermal synthesis on molybdenum substrates of 40 × 9.8 mm^2 with a thickness of 0.1 mm (99.9+ wt % Aldrich) from a synthesis mixture with the following molar oxide composition: 1:50:2500:0.5:2 $Al_2O_3/SiO_2/H_2O/Na_2O/(TPA)_2O$. The synthesis protocols and the scaleup procedure to obtain identical zeolitic coatings on 72 substrates are reported elsewhere.[5] The as-synthesized coatings were calcined and subsequently subjected to an ion exchange procedure in a 1×10^{-4} M cobalt acetate solution to obtain Co−ZSM-5 coatings.[6] A total weight of 4.5 mg of Co−ZSM-5 was obtained per plate. X-ray photoelectron spectroscopy analysis on the coatings after the post-treatment resulted in Si/Al and Co/Al ratios of approximately 26 and 0.5, respectively.

The concentrations of the components in the effluent gas were analyzed with an online Varian micro-GC (CP-4900), equipped with thermal conductivity detectors. Helium was used as a carrier gas. The analysis time was 80 s for each injection. N_2, O_2, CH_4, NO, and CO were analyzed on a molsieve 5A column (0.25 mm i.d., 10 m) operated at 175 °C and 350 kPa. C_2H_4, C_2H_6, CO_2, NH_3, and H_2O were analyzed on a poraPLOT-U column (0.25 mm i.d., 10 m) operated at 65 °C and 200 kPa. CH_3CN and CH_3OH were analyzed on a poraPLOT-U column (0.25 mm i.d., 10 m) operated at 175 °C and 150 kPa. The carbon and nitrogen mass balances were closed within 95%.

3. Results and Discussion

3.1. Flow Distribution. 3.1.1. Flow Simulation. A thick-walled screen was designed and fabricated to obtain an equal flow distribution in the HTMR compartments.[25] The elongated rectangular channels of the screen were shifted by a 90° turn relative to the rectangular reactor compartments (Figure 4). In such a geometry, the fluid is forced to flow in half a circular motion at the interface between the screen channels and the reactor compartments. In this way, local flow nonuniformities are eliminated, and the flow is smoothly distributed in all of the reactor compartments. In previous CFD studies,[25−27] the effect of different design parameters (*a*, *c*, *d*, and x^+_{up}, see Notations) of the screen on the flow nonuniformity in a downstream microstructured reactor was studied. An equation to calculate the optimum value of the key parameter of the screen (*b*, see Notation) was derived.[27] The true dimensions of the various parameters after fabrication of the HTMR sections are shown in Figure 4.

In the present study, three-dimensional CFD simulations were performed with the Fluent6.0 software to investigate the effect of the flow rate on the flow distribution in the HTMR compartments with the optimized geometry of the flow distributor (Figure 4). Only a quarter of the total system was simulated for reasons of symmetry in the two central planes perpendicular to each other. The flow simulation was performed for empty reactor compartments and with the fluid properties of air (ρ = 1.225 kg m^{-3} and $\eta = 1.79\ 10^{-5}$ Pa s). The fluid was considered as a continuous medium without slip-flow boundary conditions,[3] since the Knudsen number—based on the compartment height—is well-below the critical value of 10^{-2}. Laminar flow was assumed, because the Re_{cap} number was always below 113. The gas was assumed to be incompressible, since the Mach number[3] was well below 0.3. The temperature was fixed at 25 °C at the

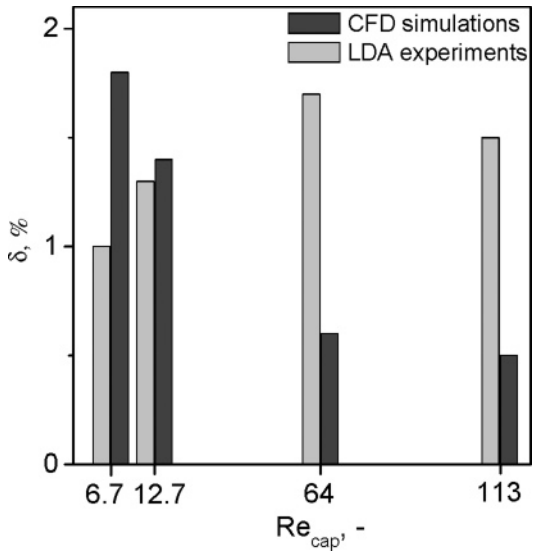

Figure 5. Flow nonuniformity in the HTMR compartments, δ (in %), from CFD simulations and LDA experiments at Reynolds numbers (Re_{cap}) of 6.7, 12.7, 64, and 113.

four flow distributor inlets, while the fluid flow was varied up to a value of 5.31 m s^{-1} ($Re_{cap} = 726$). Uniform static pressure of 101 300 Pa was specified at the four reactor compartment outlets, and the wall temperature was fixed at 500 °C. The parameter δ was introduced to quantify the degree of flow nonuniformities in the separate reactor compartments in comparison with the total average flow velocity. The parameter δ is defined as the normalized mean square deviation from the average flow, according to the following equation:

$$\delta(\%) = \frac{100}{\bar{u}}\sqrt{\frac{\sum_{i=1}^{4}(u_i - \bar{u})^2}{3}} \qquad (4)$$

where $\bar{u}$ is the total average velocity and u_i is the area-averaged velocity in reactor compartment i. Figure 5 shows the simulation results for air expressed in the percentage of the flow nonuniformity at various Re_{cap} numbers. The flow nonuniformity remained below 2% for all cases.

As described above, the LDA measurements were performed using water/PVP liquid mixtures as a flowing medium rather than air, assuming that both will behave identically for identical Reynolds numbers. This assumption was checked by repeating the CFD simulations for water/PVP mixtures. This confirmed that the fluid flow profiles in the HTMR depend only on the Reynolds number and not on the physical properties of the fluid.

3.1.2. LDA Results. The LDA analysis was performed in an identical reactor configuration, using a water/PVP mixture as a flowing medium. The flow of the water/PVP mixture through the HTMR was set in such a way that the Re_{cap} number in the LDA experiments corresponded with the Re_{cap} numbers used in the CFD study (Table 1).

The LDA measurements were performed at the outlets of the reactor compartments along the x axis (Figure 1: $z = 40$ mm and $y = 0$). The reactor compartments were not loaded with plates for a good comparison with the CFD results (section 3.1.1.). Figure 6 shows the velocity profiles obtained from the LDA experiments at four different Reynolds numbers. The parabolic velocity profiles for a laminar flow in a rectangular duct can be observed for each of the compartments. The velocity of the fluid was zero at x positions corresponding to the solid walls in between the reactor compartments. Figure 7 schematically shows the dimensions of a HTMR compartment, where

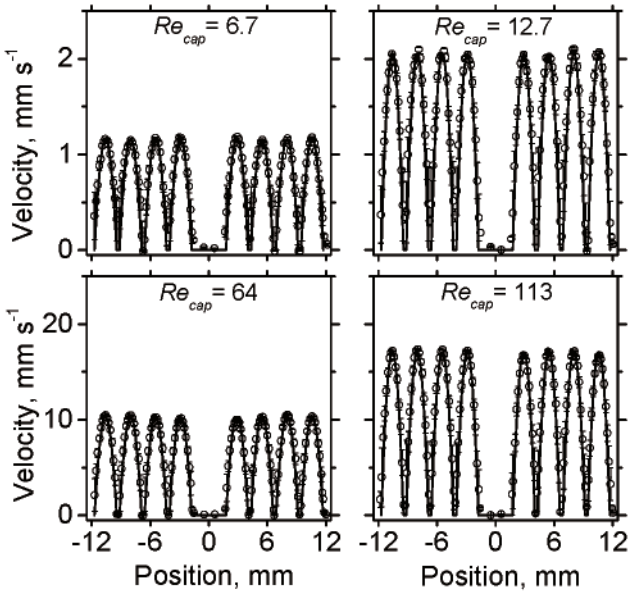

Figure 6. Velocity of the fluid flow (mm s^{-1}) in the HTMR compartments determined by LDA traverses from $x = -11.7$ to $+11.7$ mm at $z = 40$ mm, and $y = 0$ at Re_{cap} numbers of 6.7, 12.7, 64, and 113.

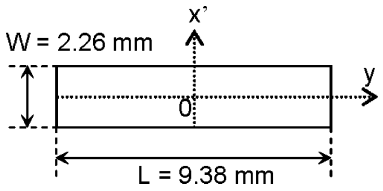

Figure 7. Schematic representation of a HTMR compartment for the theoretical determination of the parabolic velocity profile along the x' axis of a compartment for the laminar flow in a rectangular duct.

x' is specified as the x axis for an arbitrary compartment i. The exact solution for a fully developed laminar axial velocity profile for a rectangular duct i is given in Shah and London.[32] An accurate approximate solution is as follows:

$$\frac{\bar{v}_{dwn,i}}{v_{max,i}} = \left[1 - \left(\frac{x'}{0.5W}\right)^n\right]\left[1 - \left(\frac{y}{0.5L}\right)^m\right] \qquad (5)$$

where i is the compartment number 1−8, $n = 2$, and m depends on the ratio of the width (W) and length (L) of the duct, $W/L = 0.22$. For this ratio, $v_{max,i}/\bar{v}_{dwn,i} = 1.763$. The average velocity can be calculated from the maximum velocity in the compartment i, which is in the center at $x' = 0$ and $y = 0$ (Figure 7). As the LDA measurements are performed at $y = 0$, the theoretical curve along the x' axis in compartment i is as follows:

$$v_{dwn,i}(x', y = 0, z = 40 \text{ mm}) = 1.76\bar{v}_{dwn,i}\left[1 - \left(\frac{x'}{0.5W}\right)^2\right] \qquad (6)$$

The theoretical velocity profiles of eq 6 for compartments 1−8 are also shown in Figure 6, which were scaled with the maximum measured velocity in each compartment. From these maximum velocities, the corresponding average velocities in compartments 1−8 were calculated with eq 6 (Table 2). The flow nonuniformities from the LDA results were calculated with eq 4, which are shown for each Re_{cap} number in Figure 5. In all cases, the normalized mean square deviation in the flow nonuniformity was below 2%, which corresponds well with the results obtained from the CFD simulations. The LDA results indicate that the flow distributor can be used for flows with a

Table 2. Maximum and Average Velocities in the HTMR Compartments at the Various LDA Experiments (see Table 1)

Reynolds no.:	$Re_{cap} = 6.7$		$Re_{cap} = 12.7$		$Re_{cap} = 64$		$Re_{cap} = 113$	
compartment no.	$v_{max,i}$ mm s^{-1}	$\bar{v}_{dwn,i}$ mm s^{-1}	$v_{max,i}$ mm s^{-1}	$\bar{v}_{dwn,i}$ mm s^{-1}	$v_{max,i}$ mm s^{-1}	$\bar{v}_{dwn,i}$ mm s^{-1}	$v_{max,i}$ mm s^{-1}	$\bar{v}_{dwn,i}$ mm s^{-1}
1	1.16 ± 0.01	0.66 ± 0.01	2.05 ± 0.01	1.16 ± 0.01	10.47 ± 0.03	5.94 ± 0.02	17.20 ± 0.05	9.76 ± 0.03
2	1.15 ± 0.01	0.65 ± 0.01	2.10 ± 0.01	1.19 ± 0.01	10.46 ± 0.03	5.93 ± 0.02	17.38 ± 0.05	9.86 ± 0.03
3	1.17 ± 0.01	0.67 ± 0.01	2.03 ± 0.01	1.15 ± 0.01	10.28 ± 0.03	5.83 ± 0.02	17.34 ± 0.05	9.83 ± 0.03
4	1.18 ± 0.01	0.67 ± 0.01	2.04 ± 0.01	1.16 ± 0.01	10.15 ± 0.03	5.76 ± 0.02	17.24 ± 0.05	9.78 ± 0.03
5	1.18 ± 0.01	0.67 ± 0.01	2.05 ± 0.01	1.16 ± 0.01	10.01 ± 0.03	5.68 ± 0.02	16.73 ± 0.05	9.49 ± 0.03
6	1.15ep 0.01	0.65 ± 0.01	2.02 ± 0.01	1.15 ± 0.01	10.30 ± 0.03	5.84 ± 0.02	17.12 ± 0.05	9.71 ± 0.03
7	1.17 ± 0.01	0.66 ± 0.01	2.10 ± 0.01	1.19 ± 0.01	10.54 ± 0.03	5.98 ± 0.02	17.18 ± 0.05	9.75 ± 0.03
8	1.18 ± 0.01	0.67 ± 0.01	2.07 ± 0.01	1.18 ± 0.01	10.34 ± 0.03	5.86 ± 0.02	16.74 ± 0.05	9.49 ± 0.03

Re_{cap} number of about 6 up to at least 113, which corresponds to a He flow through the HTMR of approximately 60−1200 mL min^{-1} (STP).

In our previous study,[25] an optimum b/a ratio of 0.81 was found at fixed values of parameters a, c, and d of 250, 1030, and 2260 μm, respectively (Figure 4). However, due to the peculiarities of the micromachining process, the actual values of parameters a and c were 304 and 850 μm, respectively. Recently, we have shown that the optimum b/a ratio depends also on the width of the thick-walled screen channels (c) and, to a minor extent, on the height of the compartments (d) and the dimensionless length of the screen (x_{up}^+; eq 7):[27]

$$b(a,c,d,x_{up}^+) = 0.5a + 0.1678c + 0.035c\exp\left(-0.840\,x_{up}^+ + \frac{0.1986}{x_{up}^+}\right) + [(8.47\times10^{-3})c + (8.00\times10^{-6})c^2 - 1.06]\exp\left(-1.02\frac{d}{c}\right) \quad (7)$$

The dimensionless length of the screen channel ($x_{up}^+ = l_{up}/D_hRe$) is a function of the Re number. However, if the length of the screen channel is much longer than its hydraulic diameter, the third term in eq 7 becomes rather small. For example, at an x_{up}^+ of 5.0, the sum of the second and the third terms becomes $0.1683c$. With the actual values of the design parameters c and d, the fourth term in eq 7 is always much smaller compared to the first and second ones and, therefore, can be omitted. As a result, the optimum b/a value can be found by a simplified equation:

$$\frac{b}{a} = 0.5 + \frac{0.1683c}{a} \quad (8)$$

With the actual values of the design parameters, the optimum b/a value equals 0.97. A flow nonuniformity below 0.5% can be obtained in the range of b/a values between 0.91 and 1.05 as was estimated in a previous study.[27] The flow nonuniformity depends on the deviation from the optimum b/a value. This dependence can be approximated by an n-order polynomial function. The order of this function depends on the values of the design parameters; however, it is always between 1 (linear) or 2 (parabolic).[25,26] Therefore, the actual flow nonuniformity at a b/a of 0.81 is expected to be between 1.0 and 2.0%. One can see that no systematic trend is observed in the deviations between maximum velocities (Figure 6 and Table 2) at the various Re numbers. This suggests that the flow nonuniformities are caused by small variations in the experimental conditions rather than by the deviation from the optimum b/a ratio. For example, small fluctuations in the liquid flow rate within one traverse (Table 1) resulted already in deviation of ca. 3% from the average flow rate at the various Re_{cap} numbers. Furthermore, the small inaccuracy in the positioning of the LDA measurement volume at the center of the separate compartments (Appendix I) also contributed to the small deviation from the ideal flow distribution.

3.2. Temperature Distribution. The HTMR is designed for catalyst screening in the differential reactor mode, that is, at reactant conversions below 10%. The strongly exothermic ethylene oxidation was carried out over the $CuO/Al_2O_3/Al$ coatings loaded in all compartments of the HTMR. The radial (T2−T1) and axial (T3−T2) temperature gradients in the HTMR were recorded as a function of the produced reaction heat (Figure 8). The axial and radial temperature gradients remained below 3 °C in all cases. A maximum ethylene conversion of 25% was reached, which resulted in an overall heat production of 1.3 W. This is just a fraction of the heat produced by the electrical heaters (ca. 100 W). Therefore, the axial and radial temperature gradients do not depend on the heat produced in the reaction and are mainly determined by the position of the heating band (from $z = 5$ to 43 mm) relative to the interface with section VI maintained at 120 °C (see Figure 1a). Thermocouple T3 ($x =$ 0 mm and $z = 37$ mm) was positioned at the reactor centerline close to the interface with section VI, while thermocouple T1 ($z = 3$ mm and $x = 14$ mm) was positioned near the reactor outer surface close to the flow distribution header (section I, Figure 1b). An excellent transport of the heat from the electrical heaters via the molybdenum ($\lambda = 140$ W m^{-1} K^{-1}) reactor walls is achieved which allows to level off both the radial and axial temperature distribution. Therefore, temperature gradients smaller than 3 °C are expected between the reactor compartments during catalyst screening experiments.

3.3. Concentration Distribution. 3.3.1. Concentration Distribution at Process Conditions. The concentration distribution was investigated at typical process conditions for the screening of zeolitic coatings in the ammoxidation process of

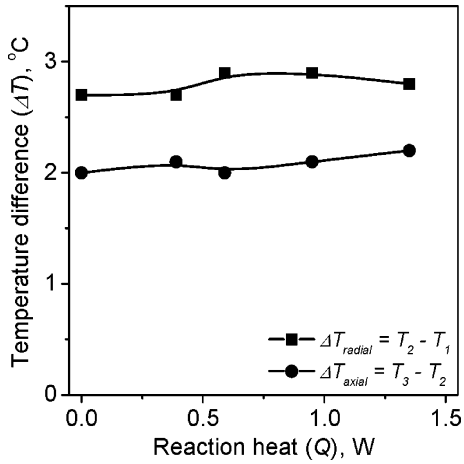

Figure 8. Radial (T2−T1) and axial (T3−T2) temperature distributions in the HTMR as a function of the produced reaction heat in ethylene oxidation over $CuO/Al_2O_3/Al$ coatings. Conditions: $T = 425$ °C, $F_v = 250$ mL min^{-1}, $[C_2H_4] = 2$ vol %, and $[O_2] = 0.5$−12 vol % in He.

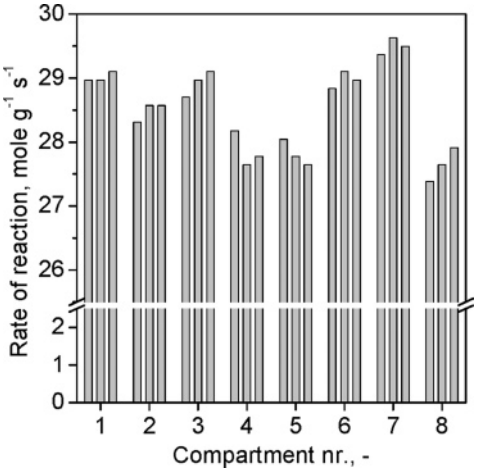

Figure 9. Rate of reaction (CH_3CN rate of formation in mol g^{-1} s^{-1}) in ethylene ammoxidation over Co−ZSM-5 coatings, which were separately tested in each of the eight reactor compartments. Conditions: $T = 425$ °C, $F_v = 250$ mL min^{-1}; and [C_2H_4], [O_2], and [NH_3] = 4 vol % in He.

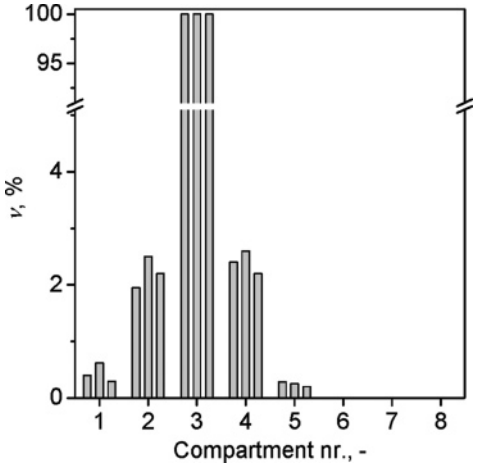

Figure 10. Cross talking noise, ν_i in the compartments of the HTMR. Compartment 3 was loaded with the active Co−ZSM-5 coatings, while the other compartments were loaded with inert titanium plates. Conditions: $T = 425$ °C; $F_v = 500$ mL min^{-1}; [C_2H_4], [O_2], and [NH_3] = 4 vol % in He.

ethylene to acetonitrile at 425 °C and a Re_{cap} number of 23.5 [250 mL min^{-1} He (STP)]. Alternately, one compartment was loaded with four Co−ZSM-5 coatings, while the other compartments were loaded with four inert titanium plates. The Co−ZSM-5 coatings were subsequently tested at the same conditions in all eight compartments separately at steady-state operation. The acetonitrile rate of formation, r (in moles of CH_3CN s^{-1}), over the Co−ZSM-5 coatings in each compartment was analyzed 3-fold, namely, three capillaries per compartment, as shown in Figure 9.

The parameter θ was introduced to quantify the degree of nonuniformities in the rates of reaction in the separate reactor compartments in comparison with the total average rate of reaction. The parameter θ is defined as the normalized mean square deviation from the average rate of reaction, according to the following equation:

$$\theta(\%) = \frac{100}{\bar{r}}\sqrt{\frac{\sum_{i=1}^{24}(r_i - \bar{r})^2}{23}} \tag{9}$$

where $\bar{r}$ is the total average rate of reaction (28.5 μmol g^{-1} s^{-1}) and r_i is the rate of reaction calculated from the C_2H_3N concentration in the sampling capillary i. The nonuniformity in the rate of reaction was 2.3% while 5-fold differences in the reaction rate (r_i) between different compartments were usually observed in a high-throughput screening of zeolitic coatings.[33] One can conclude that the difference in the reaction rate does not influence the screening results significantly. Furthermore, no systematic deviation in the reaction rate was observed either between different reactor compartments or in the position of the sampling capillary in the compartment, namely, the inner, outer, or central position. Therefore, the deviation can be attributed to small differences both in the flow conditions and in the catalytic activity of the Co−ZSM-5 coatings.

3.3.2. Cross Talking Noise in the Sampling Section. The CFD study[25] showed that the sampling of a product gas from a compartment without interference of gases from adjacent compartments can be obtained at the isokinetic suction intake by insertion of the sampling capillaries at 4 mm inside the confusor section (Figure 1e). A cross talking analysis of product gases was performed in the ethylene ammoxidation by loading the third compartment with four plates with Co−ZSM-5 coatings, while other compartments were loaded with four inert titanium plates. The percentage of the cross talking noise, ν *(%)*, in compartment i was calculated according to

$$\nu_i(\%) = 100 \times \frac{C_{CH_3CN,i}}{C_{CH_3CN,i=3}} \tag{10}$$

where $C_{CH_3CN,i}$ and $C_{CH_3CN,i=3}$ are the CH_3CN concentrations in compartment i and the third compartment, respectively. Without the interference of product gases from adjacent compartments, acetonitrile would only have been produced in the third compartment. However, an average cross talking noise of 2.3% over the three capillaries was obtained in the adjacent compartments 2 and 4 (Figure 10). The cross talking noise in the more distant first and fifth compartments was 0.5% and 0.2%, respectively. Identical results were obtained when the sampling capillaries were moved further by 2 mm inside the confusor section, confirming that back diffusion of the product gases is not an issue. This observation is in full agreement with the CFD results,[25] also indicating that the product flow to the common reactor outlets (Figure 1f) is not disturbed by the sampling capillaries.

Since the fluid flow profile in the sampling section did not affect the cross talking noise, a detailed study was performed on the physical, metallurgical, and interfacial aspects of the separate HTMR sections. The interior microstructures were produced by electrical discharge machining in which deviations in the dimensions were obtained with an accuracy of 5 μm. Subsequently, a protective alumina film of 200 nm was deposited on the molybdenum surfaces by atomic layer deposition.[6,24] Assembling of the HTMR sections II, III, V, and VI (Figure 1) was performed within an accuracy of 5 μm relative to each other. However, after cutting of the various parts from a molybdenum cylindrical bar, the surfaces were treated by conventional lathe machining, creating a surface roughness (R_a) of ca. 1.6 μm. Therefore, the interface between sections III and V (at $z = 40$ mm) can be considered as a macroporous layer through which the gas molecules can easily diffuse (Figure 1).

The interface between sections III and V was treated with carbon paste to reduce the surface roughness. Furthermore, a metal plate was inserted in the lowest cavity of the second compartment just below the sampling capillaries ($x = 6.95$ mm, Figure 2) from $z = 0$ mm to $z = 47$ mm. In this way, the cross talking noise in the second compartment was reduced from 2.3% to 0.1%. This experimental observation illustrates the importance

of smooth surface finishing in microtechnology,[34] when interfaces cannot be avoided.

4. Conclusion

The CFD design results of a microreactor consisting of eight compartments for the high-throughput screening of catalytic coatings have been experimentally validated. The performance of the reactor was checked on distributions in fluid flow, temperature, and concentration in the separate reactor compartments. The flow nonuniformities in the reactor compartments remained below 2% in the complete range of Reynolds numbers of 6−113, which was analyzed by laser Doppler anemometry. These results were in agreement with the CFD design of the low-pressure drop flow distribution header. The temperature nonuniformity between the reactor compartments was below 3 K at a maximum heat production rate of 1.3 W in ethylene oxidation at 425 °C over $CuO/Al_2O_3/Al$ coatings. With respect to concentration gradients, a deviation from the average rate of reaction of only 2.3% was obtained at realistic process conditions in the ethylene ammoxidation process over identical Co−ZSM-5 coatings in all reactor compartments. Finally, the cross talking noise of product gases in the adjacent reactor compartments could be minimized below 0.1% according to the CFD model when (1) the sampling capillaries were positioned at least 4 mm inside the reactor compartments, (2) the gas flow profile in reactor outlets was not disturbed (isokinetic suction), and (3) internal leakages between reactor compartments at interfaces of separate reactor sections were negligible.

This paper illustrates the importance and relevance of proper microreactor design prior to the actual microfabrication of the reactor's parts and their assembling. It shows that full 3D CFD design of the reactor allows for a proper evaluation of all relevant design issues (choice of reactor material, geometries, length of sampling capillaries, etc.) as well as for a detailed study of all relevant physical phenomena (flow distribution, mass and heat transport, axial disperison, etc.). The clear advantage of CFD-based microreactor design is that it allows taking full advantage of the microscale in optimizing the reaction conditions. This paper also illustrates that a proper in-depth study of the mass and heat transport taking place in the reactor provides guidelines for the actual required micromachining precision.

The results and conclusions of this paper suggest that most often it will be needed to design tailor-made microreactors for each particular application. Using off-the-shelf available parts (flow distributors, mixers, reaction compartments, etc.) for assembling a complete microreactor for a particular reaction may not provide the optimum configuration, leading to lower selectivities and yields than anticipated.

Acknowledgment

The authors would like to thank Mr. K. T. Zuidhof and Mr. R. P. Ekatpure from Eindhoven University of Technology for preparation of the $CuO/Al_2O_3/Al$ coatings and for the adaptation and calibration of the experimental setup, respectively. The financial support by the Dutch Technology Foundation (STW, Project No. EPC.5543), Shell International Chemicals B.V., Akzo Nobel Chemicals B.V., and Avantium Technologies B.V. is gratefully acknowledged.

Appendix A: Corrections and Uncertainty in Velocity Measurements

The ellipsoidal LDA measurement volume has dimensions of $1.19 \times 0.22 \times 0.22$ mm^3 (Figure 3). In order to be able to position the measurement volume as close as possible to the reactor outlets, its longitudinal axis (y axis) was aligned in an angle $1/2\gamma$ with respect to the plane of the reactor outlets, with $\gamma = 15.75°$ the angle between the two laser beams. As a result, the measured velocity component was not perfectly perpendicular to the outlet plane and a velocity correction had to be applied according to eq A1:

$$v_{\mathrm{dwn},i} = \frac{v_{\mathrm{measured}}}{\cos\left(\frac{\gamma}{2}\right)} \tag{A1}$$

Due to the finite dimensions of the measurement volume and the velocity gradients in the flow, not all measured particles have the same velocity. The velocity is determined as the average value over many particles and is assumed to be equal to the volume averaged velocity in the measurement volume. The uncertainty, s, of the local measured velocity is calculated according to equation A2:

$$s(v_{\mathrm{dwn},i}) = \frac{3\sigma}{\sqrt{N}} \tag{A2}$$

where σ is the standard deviation and $N = 20\,480$ is the number of measurements at that position.

An additional uncertainty in the local measured velocity was caused by the deviation in the positioning of the measurement volume at the outlet of the reactor compartments in the LDA traverses along the x axis ($z = 40$ mm). This deviation was experimentally determined at 0.03 mm. From eq 6, the uncertainties can be calculated with respect to the accuracy in positioning of the LDA measurement volume. This resulted in large uncertainties close to the walls of the compartments ($x' \approx \pm 1$; Figure 8) and low uncertainties at the center of the compartments ($x' \approx 0$; Figure 8). An example of the uncertainties caused by both the standard deviation (eq A1) and the deviation in positioning expressed in percentages of the local measured velocity is given in Table 3. The total uncertainty of the values in Table 2 and Figure 7 was calculated as the square root of the squared sum of the two uncertainties per measurement position.

Table 3. Uncertainties in the Local Measured Velocity (in %) at $Re_{cap} = 64$

LDA postion, x' (Figure 7)	0.02 mm ("center")	0.95 mm (close to the wall)
uncertainty in the standard deviation, σ (%)	0.084	0.25
uncertainty in the position	0.2	15
total uncertainty (%)	0.22	15

Notations

a = separation, minimum length between two neighboring downstream reactor compartments walls, mm
b = offset, distance between a top wall of the first downstream reactor compartment and a side wall of the upstream channels of the thick-walled screen, mm
c = width of the upstream channels of the thick-walled screen, mm
$C_{CH_3CN,i}$ = CH_3CN concentration in compartment i, vol %
d = height of the downstream reactor compartments, mm
F_v = total flow rate at STP conditions, m^3 s^{-1}
h = distance between the neighboring upstream channels of the thick-walled screen, mm
ΔH^0_{698K} = reaction enthalpy at 698 K, kJ mol^{-1}

Kn = Knudsen number, which is calculated with the following equation: $Kn = \lambda/l$, in which λ (m) is the mean free path of a molecule, and l (m) is the representative physical length scale

l_{up} = length of the upstream channels of the thick-walled screen, mm

l_{dwn} = length of the downstream compartments, mm

L = length of a rectangular compartment (Figure 7)

M = Mach number, which is calculated with the following equation: $M = v/a$, in which v (m s^{-1}) is the fluid flow velocity and a (m s^{-1}) the speed of sound

M_w = molar weight, g mol^{-1}

N = number of LDA measurements at a single position

Q = total produced reaction heat, W

r = rate of reaction expressed as the number of produced moles of CH_3CN per catalyst weight per second, mol g^{-1} s^{-1}

$\bar{r}$ = average rate of reaction in the eight HTMR compartments, mol g^{-1} s^{-1}

Re_{cap} = Reynolds number in inlet capillary

Re = Reynolds number in the compartments of the HTMR

s = uncertainty in the local fluid velocity measured by LDA, %

u_i = area averaged velocity in compartment i in the CFD simulation, m s^{-1}

$\bar{u}$ = average flow velocity in compartments 1−4 considered in the CFD simulations, which is calculated as follows, $\bar{u} = 1/4 \sum_{i=4}^{4} u_i$, m s^{-1}

$\bar{v}_{cap}$ = experimentally determined fluid velocity in the inlet capillary, mm s^{-1}

$v_{max,i}$ = maximum fluid velocity in compartment i at $x' = 0$ and $y = 0$ (in Figure 8), mm s^{-1}

$v_{measured}$ = fluid velocity at the position of the LDA measurement without correction, mm s^{-1}

V_m = gas molar volume at STP, 0.0224 m^3 mol^{-1}

$v_{dwn,i}$ = corrected fluid velocity at the position of the LDA measurement in compartment i, mm s^{-1}

$\bar{v}_{dwn,i}$ = average fluid velocity in compartment i, mm s^{-1}

$\bar{V}_{dwn}$ = average fluid velocity taken over all compartments, mm s^{-1}

W = width of a rectangular compartment (in Figure 7), mm. W is equal to the height of the downstream reactor compartments d (in Figure 4)

x = position at the x axis in the reactor coordinate system (Figure 1), mm

x' = position at the x' axis in an arbitrary compartment coordinate system (Figure 7), mm

x_{up}^{+} = dimensionless length of the thick-walled screen channels, which is calculated as follows: $x_{up}^{+} = \dfrac{l_{up}}{D_h \, Re}$

y = position at the y axis in the reactor coordinate system (Figure 1), mm

y_{CO_2} = mole fraction of carbon dioxide in effluent gas flow

z = position at the z axis in the reactor coordinate system (Figure 1), mm

Greek Letters

δ = normalized mean square deviation from the average flow, %

ϕ_V = total fluid flow rate in the HTMR, cm^3 s^{-1}

γ = angle between the reference and the scatter laser beam in the fluid, °

η = dynamic viscosity, mPa s

λ = heat conductivity, W m^{-1} K^{-1}

ν_i = percentage of cross talking noise in compartment i, %

ρ = density, kg m^{-3}

σ = standard deviation in the LDA measurements at a single position

θ = normalized mean square deviation from the average rate of reaction, %

Subscripts

cap = capillary

dwn = (downstream) reactor compartments

i = reactor compartment number, $1 \le i \le 8$

m = molar

up = (upstream) channels of the thick-walled screen

v = volumetric

Literature Cited

(1) Cybulski, A.; Moulijn, J. A. *Structured Catalysts and Reactors*, 2nd ed.; CRC Taylor & Francis: Oxford, U. K., 2006.

(2) Hessel, V.; Hardt, S.; Löwe, H.; Müller, A.; Kolb, G. *Chemical Micro Process Engineering*; Wiley: Belgium, 2005.

(3) Hessel, V.; Hardt, S.; Löwe, X. *Chemical Micro Process Engineering: Fundamentals, Modelling and Reactions*; Wiley: Belgium, 2004.

(4) Rebrov, E. V.; Seijger, G. B. F.; Calis, H. P. A.; de Croon, M. H. J. M.; van den Bleek, C. M.; Schouten, J. C. The Preparation of Highly Ordered Ordered Single Layer ZSM-5 Coating on Prefabricated Stainless Steel Channels. *Appl. Catal., A* **2001**, *206*, 125.

(5) Mies, M. J. M.; van den Bosch, J. L. P.; Rebrov, E. V.; Jansen, J. C.; de Croon, M. H. J. M.; Schouten, J. C. Hydrothermal Synthesis and Characterization of ZSM-5 Coatings on a Molybdenum Supports and Scale-Up for Application in Microreactors. *Catal. Today* **2005**, *110*, 38.

(6) Mies, M. J. M.; Rebrov, E. V.; Jansen, J. C.; de Croon, M. H. J. M.; Schouten, J. C. Method for the in-Situ Preparation of Zeolite Beta Crystals on a Molybdenum Substrate for Micoreactor Applications. *J. Catal* **2007**, accepted.

(7) Mies, M. J. M.; Rebrov, E. V.; Jansen, J. C.; de Croon, M. H. J. M.; Schouten, J. C. Hydrothermal Synthesis of a Continuous Zeolite Beta layer by Optimization of Time, Temperature and Heating Rate of the Precursor Mixture, Microporous Mesoporous Mater. published on-line at http://dx.doi.org/10.1016/j.micromeso.2007.02.032.

(8) Louis, B.; Kiwi-Minsker, L.; Reuse, P.; Renken, A. ZSM-5 Coatings on Stainless Steel Grids in One-Step Benzene Hydroxylation to Phenol by N_2O: Reaction Kinetics Study. *Ind. Eng. Chem. Res.* **2001**, *40*, 1454.

(9) Wunsch, R.; Fichtner, M.; Gorke, O.; Haas-Santo, K.; Schubert, K. Process of Applying Al_2O_3 Coatings in Microchannels of Completely Manufactured Microstructured Reactors. *Chem. Eng. Technol.* **2002**, *25*, 700.

(10) Ganley, J. C.; Riechmann, K. L.; Seebauer, E. G.; Masel, R. I. Porous Anodic Alumina Optimized as a Catalyst Support for Microreactors. *J. Catal.* **2004**, *227*, 26.

(11) Ismagilov, I. Z.; Ekatpure, R. P.; Tsykoza, L. T.; Matus, E. V.; Rebrov, E. V.; de Croon, M. H. J. M.; Kerzhentsev, M. A.; Schouten, J. C. Optimization of Anodic Oxidation and Cu−Cr Oxide Catalyst Preparation on Structured Aluminum Plates Processed by Electro Discharge Machining. *Catal. Today* **2005**, *105*, 516.

(12) Yang, K. S.; Jiang, Z.; Chung, J. S. Electrophoretically Al-Coated Wire Mesh and Its Application for Catalytic Oxidation of 1,2-Dichlorobenzene. *Surf. Coat. Technol.* **2003**, *168*, 103.

(13) Richardson, J. T.; Garrait, M.; Hung, J. K. Carbon Dioxide Reforming with Rh and Pt−Re Catalysts Dispersed on Ceramic Foam Supports. *Appl. Catal., A* **2003**, *255*, 69.

(14) Liguras, D. K.; Goundani, K.; Verykios, X. E. Production of Hydrogen for Fuel Cells by Catalytic Partial Oxidation of Ethanol over Structured Ni Catalysts. *J. Power Sources* **2004**, *130*, 30.

(15) Giornelli, T.; Lofberg, A.; Bordes-Richard, E. Grafting of VOx/TiO_2 Catalyst on Anodized Aluminum Plates for Structured Catalytic Reactors. *Thin Solid Films* **2005**, *479*, 64.

(16) Muraza, O.; Rebrov, E. V.; Khimyak, T.; Johnson, B. F. G.; Kooyman, P. J.; Lafont, U.; Albouy, P-A.; de Croon, M. H. J. M.; Schouten, J. C. Preparation and Characterization of Bimetallic Catalysts Supported on Mesoporous Silica Film. *Stud. Surf. Sci. Catal.* **2006**, *162*, 167.

(17) Beers, E. W.; Nijhuis, T. A.; Aalders, N.; Kapteijn, F.; Moulijn, J. A. BEA Coating of Structured Supports - Performance in Acylation. *Appl. Catal., A* **2003**, *243*, 237.

(18) Aaltonen, T.; Ritala, M.; Sajavaara, T.; Keinonen, J.; Leskelä, M. Atomic Layer Deposition of Platinum Thin Films. *Chem. Mater.* **2003**, *15*, 1924.

(19) Aaltonen, T.; Ritala, M.; Arstila, K.; Keinonen, J.; Leskelä, M. Atomic Layer Deposition of Ruthenium Thin Films from $Ru(thd)_3$ and Oxygen *Chem. Vap. Deposition* **2004**, *10*, 215.

(20) Aaltonen, T.; Ritala, M.; Sammelselg, V.; Leskelä, M. Atomic Layer Deposition of Iridium Thin Films. *J. Electrochem. Soc.* **2004**, *151*, G489.

(21) Janicke, M. T.; Kestenbaum, H.; Hagendorf, U.; Schuth, F.; Fichtner, M.; Schubert. K. The Controlled Oxidation of Hydrogen from an Explosive Mixture of Gases Using a Microstructured Reactor/Heat Exchanger and Pt/Al_2O_3 Catalyst. *J. Catal.* **2000**, *191*, 282.

(22) Chen, H. Y.; Chen, L.; Lu, Y.; Hong, Q.; Chua, H. C.; Tang, S. B.; Lin, J. Synthesis, Characterization and Application of Nano-Structured Mo_2C Thin Films. *Catal. Today* **2004**, *96*, 161.

(23) Stefanov, P.; Stoychev, D.; Valov, I.; Georgieva, A. K.; Tarinova, T. Electrochemical Deposition of Thin Zirconia Films on Stainless Steel 316. *Mater. Chem. Phys.* **2000**, *65*, 222.

(24) Kuznetsov, S. A.; Kuznetsova, S. V.; Rebrov, E. V.; Mies, M. J. M.; de Croon, M. H. J. M.; Schouten, J. C. Synthesis of Molybdenum Borides and Molybdenum Silicides in Molten Salts and Their Oxidation Behavior in an Air−Water Mixture. *Surf. Coat. Technol.* **2005**, *195*, 182.

(25) Mies, M. J. M.; Rebrov, E. V.; de Croon, M. H. J. M.; Schouten, J. C. Design of a Molybdenum High Throughput Microreactor for High Temperature Screening of Catalytic Coatings. *Chem. Eng. J.* **2004**, *101*, 225.

(26) Rebrov, E. V.; Ismagilov, I. Z.; Ekatpure, R. P.; de Croon, M. H. J. M.; Schouten, J. C. Header Design for Flow Equalization in Microstructured Reactors. *AIChE J.* **2007**, *53* (1), 28.

(27) Rebrov, E. V.; Ekatpure, R. P.; de Croon, M. H. J. M.; Schouten, J. C. Design of a Thick-Walled Screen for Flow Equalization in Microstructured Reactors. *J. Micromech. Microeng.* **2007**, *17*, 633.

(28) Mies, M. J. M.; Rebrov, E. V.; de Croon M. H. J. M.; Schouten, J. C. Inlet Section for Microreactor. Patent PCT/NL 2005000260, 2005.

(29) Delsman, E. R.; de Croon, M. H. J. M.; Elzinga, G. D.; Cobden, P. D.; Kramer, G. J.; Schouten, J. C. The Influence of Differences between Microchannels on Microreactor Performance. *Chem. Eng. Technol.* **2005**, *28*, 367.

(30) Drain, L. E. *The Laser Doppler Technique*; John Wiley Press: New York, 1980.

(31) Loseke, A. H.; Gould, R. D. A Comparison of Velocity Bias Correction Techniques in Laser-Doppler-Velocimetry. ASME Fluid Measurement and Instrumentation Forum, FED, 1991.

(32) Shah R. K.; London, A. L. *Laminar Forced Convection in Ducts*; Academic Press: New York, 1978.

(33) Mies, M. J. M.; Rebrov, E. V.; Schiepers, C. J. B. U.; de Croon, M. H. J. M.; Schouten, J. C. High Throughput Screening of Co-BEA and Co-ZSM-5 Coatings in the Ammoxidation of Ethylene to Acetonitrile in a Microstructured Reactor. *Chem. Eng. Sci.* **2007**, accepted.

(34) Picard, Y. N.; Adams, D. P.; Vasile, M. J.; Ritchey, M. B. Focused Ion Beam-Shaped Microtools for Ultra-Precision Machining of Cylindrical Components. *Precision Eng.* **2003**, *27*, 59.

Received for review August 15, 2006
Revised manuscript received January 30, 2007
Accepted January 31, 2007

IE061081W